Germanane: a Low Effective Mass and High Bandgap 2-D Channel Material for Future FETs

Ram Krishna Ghosh, Madhuchhanda Brahma, and Santanu Mahapatra, *Senior Member, IEEE*

***Abstract*— We investigate the electronic properties of Germanane and analyze its importance as 2-D channel material in switching devices. Considering two types of morphologies, namely, chair and boat, we study the real band structure, the effective mass variation, and the complex band structure of unstrained Germanane by density-functional theory. The chair morphology turns out to be a more effective channel material for switching devices than the boat morphology. Furthermore, we study the effect of elastic strain, van der Waals force, and vertical electric field on these band structure properties. Due to its very low effective mass with relatively high-energy bandgap, in comparison with the other 2-D materials, Germanane appears to provide superior performance in switching device applications.**

***Index Terms*— 2-D crystal, *ab initio* simulation, effective mass, MOSFET, real and complex band structure, tunnel field-effect transistor (TFET).**

I. Introduction

2-D MATERIALS are becoming attractive candidates for the advanced field-effect transistor (FET) channel, as it is very difficult to scale down bulk silicon thickness to a few nanometers [1]. At the same time, materials with lower effective mass are being explored to obtain high drive current and low intrinsic delay. Though the carrier mobility is extremely high in pristine graphene, the zero bandgap nature has limited its application as an electronic switch [2]. Other 2-D materials are being explored, which might have finite electronic bandgap. Monolayer transition metal chalcogenides (TMDs) (mainly MoS_2, WS_2, $MoSe_2$, WSe_2, and $MoTe_2$), topological insulators (Bi_2Se_3, Bi_2Te_3), h-BN, and so on [3]–[9] are the examples of such materials, which have been reported to be developed experimentally by simple mechanical exfoliation or chemical synthesis techniques. Some existing III–V materials (e.g., InAs) offer extremely low effective mass, but have low bandgap values that lead to different kind of leakage currents. On the other hand, the 2-D materials like TMDs show higher bandgap as well as higher effective mass. Therefore, channel material selection plays a crucial role to realize high-performance conventional or tunnel FETs (TFETs). Looking into this motivation, in this paper, we have explored the electronic properties of Germanane, which has been chemically synthesized recently [10] and promises to offer high electronic bandgap along with low effective mass. The absence of dangling bonds due to the Hydrogen saturation in Germanane can render it to be a promising channel material in device applications. We first explore the band structures and effective masses followed by the computation of complex band structure for chair and boat morphologies (Fig. 1) of unstrained Germanane. These band structure and effective mass calculations have been evaluated using Atomistix ToolKit (ATK), which uses density-functional theory (DFT) method [11]. The impact of isotropic biaxial (ε) strains on the band structure properties of both chair and boat morphologies of Germanane are then investigated. We also study the effect of vertical field and van der Waals force on the electronic properties of Germanane. All of these electronic properties are then used to assess the potential of Germanane for future FET applications.

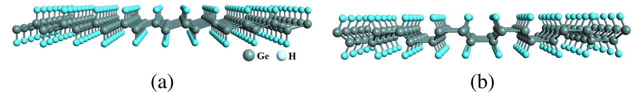

Fig. 1. Side view of the layered 2-D Germanane crystals with (a) chair and (b) boat morphologies. These are sp^3 hybridized like graphane [10].

II. Simulation Methodology

The band structure calculations of geometrically optimized Germanane have been evaluated using the ATK simulation package [11], where the structure optimization has been done by quasi-Newton scheme [12] until all the forces acting on atoms become smaller than 0.001 eV/Å. The band structure computations are based on the self-consistent DFT. The exchange correlation energies are treated within local density approximation (LDA) combining with Perdew and Zunger correlation functional and double zeta polarized basis set. We have also considered Perdew–Burke–Ernzerhof (PBE) functional under generalized gradient approximation (GGA) to compare the electronic band structure results with the LDA one. The tolerance parameter was 10^{-5} with maximum steps of 200, and a Pulay mixer algorithm [13] was used as the iteration control parameter. In addition, the k-point

Manuscript received January 8, 2014; accepted May 14, 2014. Date of publication June 3, 2014; date of current version June 17, 2014. This work was supported by the Department of Science and Technology, Government of India, under Grant SR/S3/EECE/0151/2012. The review of this paper was arranged by Editor R. Huang.

R. K. Ghosh was with the Nano-Scale Device Research Laboratory, Department of Electronic Systems Engineering, Indian Institute of Science, Bangalore 560012, India. He is now with the Pennsylvania State University, University Park, PA 16802-2700 USA (e-mail: ramki.phys@gmail.com).

M. Brahma and S. Mahapatra are with the Nano-Scale Device Research Laboratory, Department of Electronic Systems Engineering, Indian Institute of Science, Bangalore 560012, India (e-mail: madhu.brahma@gmail.com; santanu@cedt.iisc.ernet.in).

Color versions of one or more of the figures in this paper are available online at http://ieeexplore.ieee.org.

Digital Object Identifier 10.1109/TED.2014.2325136

0018-9383 © 2014 IEEE. Personal use is permitted, but republication/redistribution requires IEEE permission.
See http://www.ieee.org/publications_standards/publications/rights/index.html for more information.

TABLE I
ELECTRONIC BANDSTRUCTURE PROPERTIES OF CHAIR

DFT-	E_g (eV)	E_B (eV/atom)	Effective mass (m_0)		
			m_e	m_{hh}	m_{lh}
LDA	1.592	-2.75	0.069	0.285	0.072
GGA	1.587	-2.25	0.071	0.290	0.071

TABLE II
ELECTRONIC BANDSTRUCTURE PROPERTIES OF BOAT

DFT-	E_g (eV)	E_B (eV/atom)	Effective mass (m_0)					
			[100]		[010]		[110]	
			m_e	m_h	m_e	m_h	m_e	m_h
LDA	1.390	-2.56	0.807	0.505	0.107	0.158	0.139	0.193
GGA	1.391	-2.02	0.811	0.509	0.104	0.157	0.141	0.195

sampling of 27×27×1 grid was used with a mesh cutoff energy of 10 Hartree. In the case of monolayer sheets, we used a supercell with a 15-Å vacuum region along the c-axis (keeping the lattice parameters a and b same as bulk) to make it an isolated 2-D layer, where the different lattice parameters of both the structures have been considered from [10] and [14]. To explore the elastic strain effect in our study, the isotropic biaxial (ε) strain is applied on the optimized structures of Germanane by scaling the lattice constant of Germanane by an amount $\varepsilon = (a - a_0)/a_0$, where a_0 and a are the lattice constants for the unit cell of the unstrained and strained Germanane, respectively. In our discussion later in this paper, we will denote compressive and tensile strains by negative and positive values of ε, respectively.

III. RESULTS AND DISCUSSION

A. Unstrained Germanane

Before going into the details of electronic properties, we first have to understand the energetic stability of these structures. For this, we have computed the binding energies of these morphologies where the binding energy is defined as $E_B = E_{\text{total}} - n_{\text{Ge}}E_{\text{Ge}} - n_H E_H$ in which E_{total} is the total energy of different conformations, E_{Ge} and E_H are the spin-polarized energies of Ge and H atoms, and n_{Ge} and n_H are the number of atoms in those structural conformations [15]. From the calculated binding energies, as shown in Tables I and II, we can find that both the structures are stable, whereas chair is more stable than the boat one and that is also illustrated in [14] and [15] for Germanane as well as for silicane.

Now, the calculated electronic band structure of unstrained monolayer Germanane and the corresponding projected density of states (PDOS) are shown in Fig. 2. It is seen from Fig. 2(a) that, in case of chair morphology, both the conduction band minimum (CBM) and valence band maximum (VBM) occur at the Γ point, thereby exhibiting direct bandgap. It can also be seen that the valence band maxima at the Γ consists of a heavy hole (hh) and a light hole (lh) bands. The boat morphology also exhibits direct bandgap at the Γ point [Fig. 2(b)]; however, both band extrema do not have parabolic nature as the chair one. It is seen that both LDA and GGA produces almost the same energy bandgap values (Tables I and II), which are consistent with other theoretical

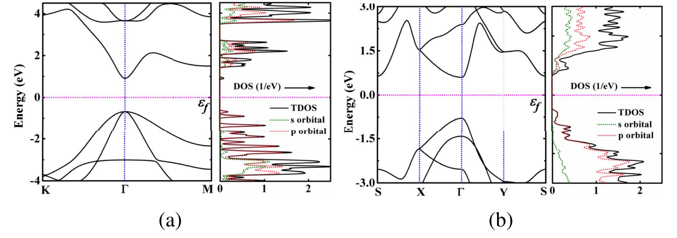

Fig. 2. Energy band structure and PDOS of Germanane (a) chair and (b) boat as calculated by DFT-LDA calculations.

calculations as well as experimental data reported in [10] and [16]. It can also be understood from the PDOS that the total density of states (TDOS) is determined by the p-orbital in each of the morphologies of Germanane.

We have also calculated the contour plots of the lowest conduction band and highest valence bands in the Brillouin zones of both the chair (Fig. 3) and boat (Fig. 4) morphologies. The contour plot serves as a convenient way to determine the anisotropic nature of the effective masses at various points of the Brillouin zone. In the band structure of chair morphologies, it is observed that there are two valence bands meeting at the Γ point. Both these valence bands have been taken into consideration for our contour plot calculations, and they will be referred as V_{hh} and V_{lh}. The contour plot analysis of Germanane chair reveals that the maximum values of the bottom conduction band occur at K, K′ valleys, the corner of the Brillouin zone, and minimum values are at the Γ point. Since the minima of the conduction band are isotropic with circular isocontours in the close vicinity of the Γ point, so the effective mass of electron near the Γ point is direction independent. However, as we move far away from the Γ point to the secondary minima at M, the contours become anisotropic, and thus the effective masses become strongly direction dependent. In case of contour plots of V_{hh} and V_{lh} of Germanane chair, it is seen that the maxima of both the valence bands at the Γ point are isotropic but become anisotropic at the K, K′ valleys, which means directionally independent hole effective masses at the valence band maxima. Both the electron and hole effective masses of chair structure are listed in Table I. On the other hand, the contour plot of the lowest conduction band of boat morphology shows that the minima at the Γ point are highly anisotropic due to their elliptical nature. It is further noticed that the maximum of the valence band at Γ point is also highly anisotropic leading to directional dependence of the effective mass at that point. In Table II, we have listed the bandgap and effective mass values of boat structure along three crystallographic directions [100], [010], and [110]. From the table, it is seen that the electron and hole effective masses of boat are the least along both [010] and [110] directions. So, to obtain higher mobility in case of boat morphologies, we have to cut the crystal along the directions where effective mass acquires the least value. However, in the case of chair morphologies, the very low effective mass is direction independent leading to uniform and much higher mobility in all directions. Thus, fabricating devices out of chair morphologies of Germanane will be comparatively simpler and easier.

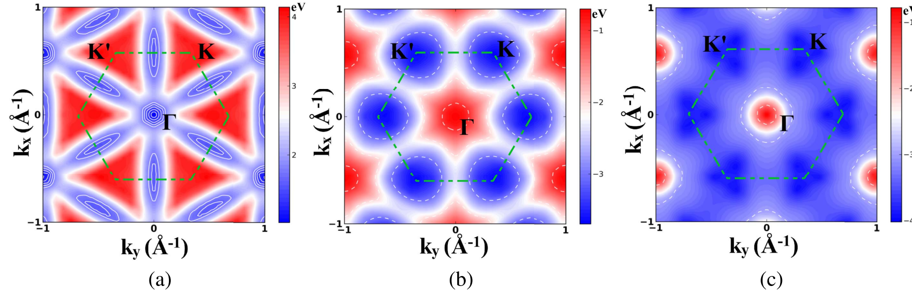

Fig. 3. Contour plot of (a) lowest conduction band and highest valence bands, (b) V_{hh}, and (c) V_{lh} in the hexagonal Brillouin zone of Germanane chair as obtained by DFT-LDA calculations.

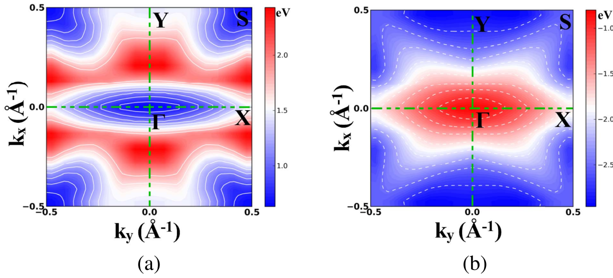

Fig. 4. Contour plot of (a) lowest conduction band and (b) highest valence bands of Germanane boat morphology by DFT-LDA calculation.

From Table III, where we compare the energy bandgap and carrier effective masses of different materials, it can be seen that the electronic bandgap of TMDs and other regular 2-D materials has much higher effective masses along with their higher bandgap. Whereas, we can see from Table I that Germanane chair has 5–10 times smaller electronic effective mass in comparison with these typical 2-D materials. Thus, Germanane chair can produce much higher carrier mobility, which eventually increases the ON-current performances of the switching devices. Again, it is seen from Table III that some of III–V materials (e.g., InAs, GaSb, InSb, different III–V alloys, etc.), which are commonly used in high mobility switching devices in recent technologies, have much smaller electronic effective masses; however, their bandgaps are also quite less, which eventually increases various leakage current in the devices. However, we can find that the effective mass of Germanane is comparable with the traditional III–V materials, while it also provides much higher bandgap value that can reduce the OFF-state current. Thus, Germanane can be a strong alternative choice of 2-D channel material that can give desired ON–OFF ratio in future MOSFET applications.

B. Complex Band Structure

During the process of tunneling through a bandgap, a carrier physically travels in an evanescent mode. As a result, its wavevector becomes imaginary along that tunneling direction within the forbidden gap region and that eventually constitutes the complex band structure. Thus, it is necessary to study the complex band structure of any channel material for a deeper understanding of band-to-band tunneling (BTBT) process in tunneling devices like TFETs [6], [25], [27]. Fig. 5(a) shows

TABLE III

BANDGAP AND EFFECTIVE MASS OF DIFFERENT CONVENTIONAL 2-D AND III–V MATERIALS

Material	E_g (eV)	Effective mass(m_0)	
		m_e	m_{hh}
Pristine Graphene[a]	0.0	0.0	0.0
1L - MoS_2[b]	1.78 - 1.89	0.58 - 0.60	0.66
1L - $MoSe_2$[c]	1.49 - 1.58	0.60	0.71
1L - $MoTe_2$[d]	1.10 -1.15	0.60-0.62	0.74-0.76
1L - WS_2[e]	1.90 - 2.05	0.35	0.46
1L - WSe_2[f]	1.49 - 1.60	0.53	0.52
Graphane[g]	3.6, 5.4	1.04, 1	0.8
Boron Nitride[h]	4.3 - 4.56	0.95 - 1	0.9
1L - SiC[i]	2.57	0.41	0.48
1L - ZnO[j]	1.68	0.253	0.374(lh), 0.793(hh)
InAs[k]	0.35	0.023	0.029(lh), 0.6(hh)
GaSb[l]	0.72	0.041	0.05(lh), 0.4(hh)
InSb[m]	0.17	0.014	0.015(lh), 0.43(hh)
InP[n]	1.35	0.08	0.09(lh), 0.6(hh)
GaAs[o]	1.42	0.063	0.082(lh), 0.51(hh)
$In_{0.53}Ga_{0.47}As$[p]	0.75	0.041	0.051(lh), 0.46(hh)

The corresponding values have been taken from the following Ref.
a: [2], b-f: [3]- [6], [17], g: [18]- [19], h: [20]- [21], i: [22] j: [22], k-p: [23], [24]

TABLE IV

COMPARISON OF ξ_I AND λ WITH HEXAGONAL TMDS

	Germanane chair	MoS_2	$MoSe_2$	$MoTe_2$	WS_2	WSe_2
ξ_I (Vnm^{-1})	0.29	1.02	0.85	0.81	1.25	0.96
λ (nm)	0.35	0.38	0.45	0.72	0.42	0.43

ξ_I is the "least action integral" and λ is the natural length scale and has been calculated by considering 2nm thick HfO_2 ($\varepsilon_{ox} = 25\varepsilon_0$) as a gate dielectric. The ξ_I and λ values of TMDs have been taken from Ref. [6].

the complex bands of chair morphology in which we can see that it produces a continuous band that connects the conduction band with the light hole (lh) bands. As the curvature of the complex band depends on the effective mass in a manner $\kappa \propto \sqrt{m^*}$ [29] (where κ is the imaginary wavevector and m^* is the effective mass), thus nearly same electron as well as hole effective mass from parabolic bands can only produce the continuous bands; otherwise, the electronic (hole) nature of complex band remains at the valence (conduction) band edge, and that is unphysical as at the valence (conduction) band edge, the band will be determined only by hole (electron) wavevector (real part). Therefore, the wrapping nature in

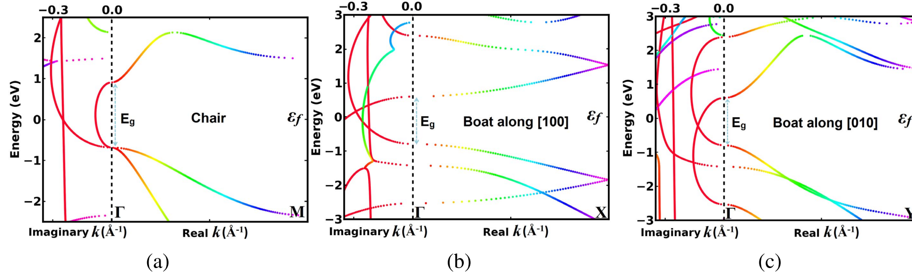

Fig. 5. Complex and real bands of monolayer Germanane for (a) chair and boat morphologies, where we have shown two crystallographic orientations (b) along [100] and (c) along [010] for boat structure. The color coding of the k-values applies to both real and imaginary parts of the band structure to make it easier to realize where the complex bands are attached to the real ones. E_g and E_f are bandgap and the Fermi level, respectively.

Germanane chair can only be seen between electron and light hole (lh) bands like III–V materials [26]. On the other hand, we can see from Fig. 5(b) and (c) that there is crossing of valence band and conduction band branches inside the forbidden bandgap of the boat structure in any crystallographic orientations as the band extrema does not have parabolic nature. Therefore, it can be claimed that the chair morphology of Germanane will prove to be more effective materials for TFETs than their boat counterpart because of wrapping of complex bands, which will ultimately result in direct BTBT with increased transmission rate.

Though a rigorous nonequilibrium Green's function-based numerical simulation is needed to study TFET performance, however, here, we will present a simplified way to understand the importance of Germanane chair as TFET channel materials. Using the Wentzel–Kramers–Brillouin approximation, the direct tunneling probability for the BTBT process can be approximated as [27], [28] $T_{\text{BTBT}} = \exp\{-(2/q\xi)\int_0^{E_g} k(E)\, dE\} \equiv \exp\{-\xi_I/\xi\}$, where q is the electronic charge, ξ the electric field, $E = 0$ is the valence band edge, $E = E_g$ is the conduction band edge, $k(E)$ the magnitude of the imaginary wavevector with least action for tunneling within the forbidden gap, and $\xi_I = 2/q(\int_0^{E_g} k(E)dE)$ is basically the least action integral, which is an intrinsic property of the material. Thus, ξ_I should be lower to increase the T_{BTBT} in any applied electric field, controlled by a third terminal (the gate) in TFET applications. The possible way to reduce this ξ_I value is by decreasing the bandgap, which eventually increases leakage current. Alternatively, by reducing the carrier effective masses, we can decrease the ξ_I value as the curvature of complex band decreases with the decrease of effective mass. When we calculate the ξ_I value, we can find that it is 0.29 V nm^{-1} for Germanane chair, which is three to four times smaller than the TMDs (Table IV). Thus, Germanane chair can lead to much higher tunneling probability for a given electric field. Now, as the electric field calculated from the surface potential profile of a TFET can be given by $\xi \propto 1/\lambda$, where λ is the screening length, it is also necessary to check the λ of that device to understand the ON-current performance of a TFET. In case of double-gate TFET, this λ can be expressed as [30] $\lambda = [(\varepsilon_{\text{ch}}/2\varepsilon_{\text{ox}})\{1 + (\varepsilon_{\text{ox}}/4\varepsilon_{\text{ch}})(t_{\text{ch}}/t_{\text{ox}})\}t_{\text{ch}}t_{\text{ox}}]^{1/2}$, where, ε_{ch} and ε_{ox} are the channel and oxide dielectric constants, respectively. As can be understood, T_{BTBT} is then controlled by the product $\lambda \times \xi_I$. Thus, higher λ reduces the tunneling probability. As λ is a function of channel dielectric constant, so we have also computed the static dielectric constant $\text{Re}[\varepsilon(\omega = 0)]$. In this computation, we use DFT-LDA and double zeta double polarized basis set along with a mesh cutoff energy of 75 Hartree and keeping the same the k-point sampling as earlier. The Kubo–Greenwood formula has been used to calculate the susceptibility tensor $(\chi(\omega))$ [31], [32], which is related to the dielectric constant as $\varepsilon(\omega) = (1 + \chi(\omega))\,\varepsilon_0$, where ε_0 is the vacuum permittivity. From this analysis, we get $\varepsilon_{\text{ch}} = 4.13\varepsilon_0$ that eventually gives $\lambda = 0.35$ nm for the inherent ultrathin Germanane chair if we consider 2-nm thick HfO_2 ($\varepsilon_{\text{ox}} = 25\varepsilon_0$) as a gate dielectric. Whereas ultrathin-body GaAs, having 5-nm thickness, provides a λ of 2.4 nm, and that is seven times higher than the monolayer Germanane chair, which has a comparable λ as the monolayer TMDs (Table IV). Thus, much lesser value of the product $\lambda \times \xi_I$ provides a high transmission rate, which increases the ON-current performances in Germanane-based TFETs.

C. Effect of Elastic Strain

One of the most recent and successful method for improving the carrier mobility and ON-current performance in the devices is the strain-dependent modulation of the transport properties of channel material [33]. Keeping that in mind, in the following section, we have investigated the impact of strain on the electronic properties of Germanane. Fig. 6 shows the effect of in-plane isotropic biaxial ε ($\varepsilon_{xx} = \varepsilon_{yy}$) strain on the real band structure of Germanane chair and boat morphologies. It appears that with the application of elastic strain, the nature of band structure undergoes a direct to indirect bandgap transition in deep compressive (for chair) and tensile (for boat) zone. However, the band valleys for the direct bandgap at Γ remains unaltered for both the cases, only the overall conduction (valence) band moves down (up). From Fig. 7(a), we can see that the direct bandgap of Germanane chair decreases with the increase of tensile strain, whereas it increases with the increase of compressive strain. Moreover, the indirect bandgap increases very slowly with the increase of compressive strains after the direct to indirect transition at -4.8%. In Fig. 7(b), we have shown the bandgap variation of boat structure. Here, we can see that direct bandgap increases with the increase

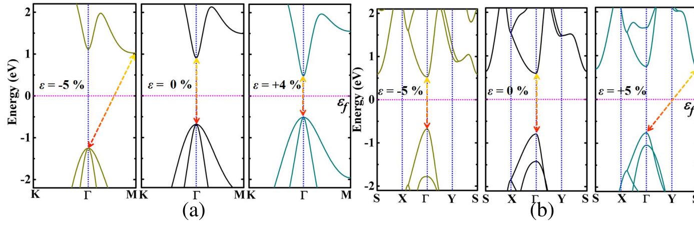

(c)

(d)

Fig. 6. Real band structure of Germanane (a) chair and (b) boat, and the partial charge densities of CBM and VBM at Γ for both (c) chair and (d) boat morphologies under different strain conditions. The isovalue is 0.06 e/Å^3. The phase shift in isosurfaces caused due to the direct–indirect bandgap transition.

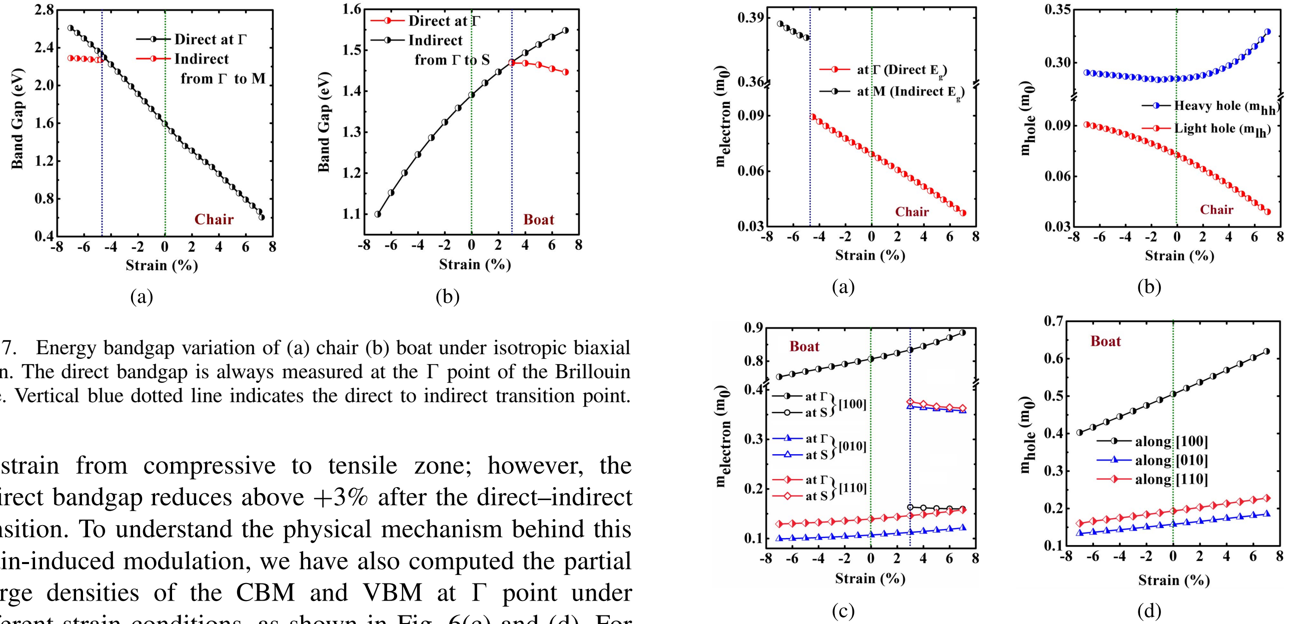

Fig. 7. Energy bandgap variation of (a) chair (b) boat under isotropic biaxial strain. The direct bandgap is always measured at the Γ point of the Brillouin zone. Vertical blue dotted line indicates the direct to indirect transition point.

Fig. 8. Electron and hole effective mass variation for (a) and (b) chair and (c) and (d) for boat along three crystallographic directions under biaxial strain. Vertical blue dotted line indicates the direct to indirect transition.

of strain from compressive to tensile zone; however, the indirect bandgap reduces above +3% after the direct–indirect transition. To understand the physical mechanism behind this strain-induced modulation, we have also computed the partial charge densities of the CBM and VBM at Γ point under different strain conditions, as shown in Fig. 6(c) and (d). For the unstrained chair structure (0%), it is seen that the CBM and VBM charge densities are highly localized at the Ge atoms and Ge–Ge bonds, respectively [Fig. 6(a)]. However, if we move from compressive to tensile region, Fig. 6(c) shows that the position of CBM charge densities remains nearly same; however, the VBM charge densities spread out from its highly localized position in the tensile strain region. Due to this, bandgap at Γ reduces with the application of tensile strain and that shows a very good agreement with [35]. On the other hand, the opposite thing happens for boat structure, where the CBM charge densities becomes more and more localized on Ge atoms [Fig. 6(d)] along with VBM on bonds in tensile strain region, which eventually increases the bandgap at Γ. Fig. 8 shows the electron (m_e) as well as hole (m_h) effective mass variation in both the morphologies of Germanane with the strain as measured at the band extrema. It is seen from Fig. 8(a) and (b) that as the value of strain is gradually increased from compressive to tensile zone for Germanane chair sheets, the electron effective mass as well as light hole effective mass (m_{lh}) at Γ decreases in a same manner and reaches as low as 0.03 m_0 at +7% strain. However, the heavy hole effective mass (m_{hh}) measured at valence band maxima increases with the increase of tensile strain in Germanane chair sheet, it shows a slow increment in tensile strain region, whereas it remains almost invariant in compressive strain region. In Germanane boat, both m_e and m_h at Γ gradually increase with the increase of strain from −ve to +ve region. It can also be seen that m_e decreases very slowly at S after the direct to indirect transition. It is found that the nature of complex bands remained unaltered with the application of strains though the values of ξ_I change. Overall, the reduction of E_g, m_e, m_{lh} and ξ_I with the application of tensile strain becomes more effective in the case of Germanane chair sheets to increase the ON-current performance in MOSFETs and TFETs.

D. Effect of Van Der Waals Force and Vertical Electric Field

We have also explored the band structure of bilayer chair morphology using both DFT-LDA and GGA methods (red) to understand the effect of van der Waals force. To incorporate the long-range van der Waals correction in interlayer interaction within GGA approximation, we have also included Grimme's DFT-D2 functional with $S_6 = 0.75$ under

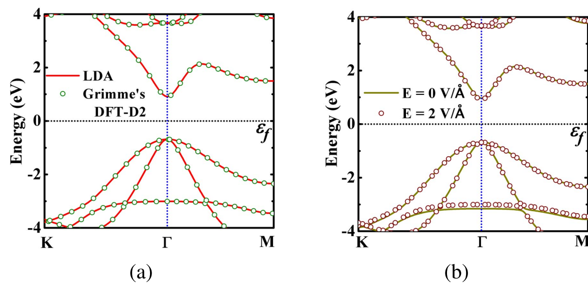

Fig. 9. (a) Real band structure by both DFT-LDA and Grimme's DFT-D2 methods. (b) Vertical electric field effect on monolayer chair.

PBE functional. After relaxing the atomic structure in all three directions, we have seen an interlayer distance of ∼5.5Å within the layers. When we calculate the band structure by both the methods, we have seen that both have given exactly same bandstructure as the monolayer one [Fig. 9(a)]. It can be understood that the interlayer interaction is extremely weak due to the hydrogen saturation of the out-of-plane valencies of Germanene, and thus the direct nature of the band structure remains unaltered unlike bilayer TMDs, where bandgap shows indirect nature [3]–[6]. We can also expect that the band structure will always show same if we further increase the number of layers. Therefore, it gives an advantage to get desired thickness of channel width just by increasing the number of Germanane layers without deforming the electronic properties. We have also studied vertical electric field effect on chair morphology. Unlike Germanene, which opens a bandgap in vertical electric field [34], its bandgap as well as band extrema also remains invariant even under high vertical electric field [Fig. 9(b)] due to its hydrogen saturation, which gives advantage as electric field is relatively high in TFET application.

IV. Conclusion

We have studied both boat and chair morphologies of Germanane using DFT, and found out that Germanane chair has both higher energy bandgap as well as very low carrier effective mass. The band structure parameters have also been studied under the effect of isotropic biaxial strain, vertical electric field, and van der Waals interaction for multilayer structures, and in each case, it has been found that Germanane chair is more effective for switching device applications.

References

[1] Y. Taur and T. H. Ning, *Fundamentals of Modern VLSI Devices*, 2nd ed. Cambridge, U.K.: Cambridge Univ. Press, 2009.

[2] K. S. Novoselov *et al.*, "Electric field effect in atomically thin carbon films," *Science*, vol. 306, no. 5696, pp. 666–669, Oct. 2004.

[3] B. Radisavljevic, A. Radenovic, J. Brivio, V. Giacometti, and A. Kis, "Single-layer MoS_2 transistors," *Nature Nanotechnol.*, vol. 6, no. 3, pp. 147–150, Mar. 2011.

[4] H. Fang, S. Chuang, T. C. Chang, K. Takei, T. Takahashi, and A. Javey, "High-performance single layered WSe_2 p-FETs with chemically doped contacts," *Nano Lett.*, vol. 12, no. 7, pp. 3788–3792, Jun. 2012.

[5] L. Liu, S. Bala Kumar, Y. Ouyang, and J. Guo, "Performance limits of monolayer transition metal dichalcogenide transistors," *IEEE Trans. Electron Devices*, vol. 58, no. 9, pp. 3042–3047, Sep. 2011.

[6] R. K. Ghosh and S. Mahapatra, "Monolayer transition metal dichalcogenide channel based tunnel transistor," *IEEE J. Electron Devices Soc.*, vol. 1, no. 10, pp. 175–180, Oct. 2013.

[7] D. Kong *et al.*, "Few-layer nanoplates of Bi_2Se_3 and Bi_2Te_3 with highly tunable chemical potential," *Nano Lett.*, vol. 10, no. 6, pp. 2245–2250, May 2010.

[8] D. Golberg *et al.*, "Boron nitride nanotubes and nanosheets," *ACS Nano*, vol. 4, no. 6, pp. 2979–2993, May 2010.

[9] K. S. Novoselov *et al.*, "Two-dimensional atomic crystals," *PNAS*, vol. 102, no. 30, pp. 10451–10453, Jul. 2005.

[10] E. Bianco, S. Butler, S. Jiang, O. D. Restrepo, W. Windl, and J. E. Goldberger, "Stability and exfoliation of germanane: A germanium graphane analogue," *ACS Nano*, vol. 7, no. 5, pp. 4414–4421, Mar. 2013.

[11] Atomistix ToolKit (ATK). *QuantumWise Simulator* [Online]. Available: http://www.quantumwise.com/

[12] D. Sheppard, R. Terrell, and G. Henkelman, "Optimization methods for finding minimum energy paths," *J. Chem. Phys.*, vol. 128, no. 13, pp. 134106-1–134106-11, Apr. 2008.

[13] P. Pulay, "Convergence acceleration of iterative sequences. The case of SCF iteration," *Chem. Phys. Lett.*, vol. 73, no. 2, pp. 393–398, Jul. 1980.

[14] P. M. Houssa, E. Scalise, K. Sankaran, G. Pourtois, V. V. Afanas'ev, and A. Stesmans, "Electronic properties of hydrogenated silicene and germanene," *Appl. Phys. Lett.*, vol. 98, no. 22, pp. 223107-1–223107-3, Jun. 2011.

[15] Y. Ding and Y. Wang, "Electronic structures of silicene fluoride and hydride," *Appl. Phys. Lett.*, vol. 100, no. 8, pp. 083102-1–083102-4, Feb. 2012.

[16] K. J. Koski and Y. Cui, "The new skinny in two-dimensional nanomaterials," *ACS Nano*, vol. 7, no. 5, pp. 3739–3743, May 2013.

[17] A. Ramasubramaniam, "Large excitonic effects in monolayers of molybdenum and tungsten dichalcogenides," *Phys. Rev. B*, vol. 86, no. 11, pp. 1098–0121, Sep. 2012.

[18] O. Pulci, P. Gori, M. Marsili, V. Garbuio, R. D. Sole, and F. Bechstedt, "Strong excitons in novel two-dimensional crystals: Silicane and germanane," *Europhys. Lett.*, vol. 98, no. 3, p. 37004, May 2012.

[19] B. Gharekhanlou and S. Khorasani, "Current-voltage characteristics of graphane p-n junctions," *IEEE Trans. Electron Devices*, vol. 57, no. 1, pp. 209–214, Jan. 2010.

[20] X. Blase, A. Rubio, S. G. Louie, and M. L. Cohen, "Quasiparticle band structure of bulk hexagonal boron nitride and related systems," *Phys. Rev. B*, vol. 51, no. 11, p. 6868, Mar. 1995.

[21] B. Huang and H. Lee, "Defect and impurity properties of hexagonal boron nitride: A first-principles calculation," *Phys. Rev. B*, vol. 86, no. 24, p. 245406, Dec. 2012.

[22] G. Mukhopadhyay and H. Behera, "Graphene and some of its structural analogues: Full-potential density functional theory calculations," *World J. Eng.*, vol. 10, no. 1, pp. 39–48, Mar. 2013.

[23] *NSM Archive-Physical Properties of Semiconductors* [Online]. Available: http://www.ioffe.ru/SVA/NSM/Semicond/

[24] Y. Takeda, A. Sasaki, Y. Imamura, and T. Takagi, "Electron mobility and energy gap of $In_{0.53}Ga_{0.47}As$ on InP substrate," *J. Appl. Phys.*, vol. 47, no. 12, pp. 5405–5408, Dec. 1976.

[25] M. Luisier and G. Klimeck, "Simulation of nanowire tunneling transistors: From the Wentzel-Kramers-Brillouin approximation to full-band phonon-assisted tunneling," *J. Appl. Phys.*, vol. 107, no. 8, pp. 084507-1–084507-6, Apr. 2010.

[26] Y. C. Chang, "Complex band structures of zinc-blende materials," *Phys. Rev. B*, vol. 25, no. 2, pp. 605–619, Jan. 1982.

[27] R. K. Ghosh and S. Mahapatra, "Proposal for graphene-boron nitride heterobilayer based tunnel FET," *IEEE Trans. Nanotechnol.*, vol. 12, no. 5, pp. 665–667, Jul. 2013.

[28] S. M. Sze and K. K. Ng, *Physics of Semiconductor Devices*, 3rd ed. Hoboken, NJ, USA: Wiley, 2007.

[29] X. Guan, D. Kim, K. C. Saraswat, and H.-S. P. Wong, "Complex band structures: From parabolic to elliptic approximation," *IEEE Electron Device Lett.*, vol. 32, no. 9, pp. 1296–1298, Sep. 2011.

[30] K. Suzuki, T. Tanaka, Y. Tosaka, H. Horie, and Y. Arimoto, "Scaling theory for double-gate SOI MOSFET's," *IEEE Trans. Electron Devices*, vol. 40, no. 12, pp. 2326–2329, Dec. 1993.

[31] W. A. Harrison, *Solid State Theory*. New York, NY, USA: McGraw-Hill, 1970.

[32] R. M. Martin, *Electronic Structure*. Cambridge, U.K.: Cambridge Univ. Press, 2004.

[33] Y. Sun, S. E. Thompson, and T. Nishida, *Strain Effect in Semiconductors: Theory and Device Applications*. New York, NY, USA: Springer-Verlag, 2010.

[34] Z. Ni *et al.*, "Tunable bandgap in silicene and germanene," *Nano Lett.*, vol. 12, no. 1, pp. 113–118, Nov. 2011.

[35] Y. Li and Z. Chen, "Tuning electronic properties of germanane layers by external electric field and biaxial tensile strain: A computational study," *J. Phys. Chem. C*, vol. 118, no. 2, pp. 1148–1154, Dec. 2013.

Ram Krishna Ghosh received the M.Sc. degree in physics from IIT Madras, Chennai, India, in 2008, and the Ph.D. degree from the Department of Electronic Systems Engineering, Indian Institute of Science, Bangalore, India, in 2013.

He is currently a Post-Doctoral Fellow with the Department of Electrical Engineering, Pennsylvania State University, University Park, PA, USA.

Madhuchhanda Brahma received the M.Tech. degree in VLSI design from Bengal Engineering and Science University, Kolkata, India, in 2013.

She is currently a Project Associate with the Nano-Scale Device Research Laboratory, Department of Electronic Systems Engineering, Indian Institute of Science, Bangalore, India. Her current research interests include computational study of 2-D layered materials and tunneling FETs.

Santanu Mahapatra (M'08–SM'10) received the Ph.D. degree from the Swiss Federal Institute of Technology Lausanne, Lausanne, Switzerland, in 2005.

He is currently an Associate Professor with the Indian Institute of Science, Bangalore, India.

Prof. Mahapatra was a recipient of the 2012 Ramanna Fellowship in the discipline of electrical sciences from the Department of Science and Technology, Government of India.